Published in final edited form as:
J Neurosci Methods. 2010 May 15; 188(2): 258–269. doi:10.1016/j.jneumeth.2010.02.019.

Establishing a model spinal cord injury in the African green monkey for the preclinical evaluation of biodegradable polymer scaffolds seeded with human neural stem cells

Christopher D. Pritchard[a,c,*], **Jonathan R. Slotkin**[b], **Dou Yu**[c], **Haining Dai**[d], **Matthew S. Lawrence**[e], **Roderick T. Bronson**[f], **Francis M. Reynolds**[g], **Yang D. Teng**[c], **Eric J. Woodard**[h], and **Robert S. Langer**[a]

Christopher D. Pritchard: cpritcha@mit.edu

[a]Department of Chemical Engineering, Massachusetts Institute of Technology, Cambridge, MA, USA

[b]Washington Brain & Spine Institute, Washington, DC, USA

[c]Department of Neurosurgery, Brigham and Women's Hospital, Boston, MA, USA

[d]Department of Neuroscience, Georgetown University Medical Center, Washington, DC, USA

[e]RxGen, Inc., Hamden, CT, USA

[f]Department of Pathology, Harvard Medical School, Boston, MA, USA

[g]InVivo Therapeutics Corporation, Cambridge, MA, USA

[h]Department of Neurosurgery, New England Baptist Hospital, Boston, MA, USA

Abstract

Given the involvement of post-mitotic neurons, long axonal tracts and incompletely elucidated injury and repair pathways, spinal cord injury (SCI) presents a particular challenge for the creation of preclinical models to robustly evaluate longitudinal changes in neuromotor function in the setting in the presence and absence of intervention. While rodent models exhibit high degrees of spontaneous recovery from SCI injury, animal care concerns preclude complete cord transections in non-human primates and other larger vertebrate models. To overcome such limitations a segmental thoracic (T9–T10) spinal cord hemisection was created and characterized in the African green monkey. Physiological tolerance of the model permitted behavioral analyses for a prolonged period post-injury, extending to predefined study termination points at which histological and immunohistochemical analyses were performed. Four monkeys were evaluated (one receiving no implant at the lesion site, one receiving a poly(lactide-co-glycolide) (PLGA) scaffold, and two receiving PLGA scaffolds seeded with human neural stem cells (hNSC)). All subjects exhibited Brown-Séquard syndrome 2 days post-injury consisting of ipsilateral hindlimb paralysis and

*Corresponding author at: Room E25-342, 45 Carleton St., Cambridge, MA02142, USA. Tel.: +1 212 729 8988; fax: +1 617 258 8827.

Appendix A. Supplementary data: Supplementary data associated with this article can be found, in the online version, at doi: 10.1016/j.jneumeth.2010.02.019.

contralateral hindlimb hypesthesia with preservation of bowel and bladder function. A 20-point observational behavioral scoring system allowed quantitative characterization of the levels of functional recovery. Histological endpoints including silver degenerative staining and Iba1 immunohistochemistry, for microglial and macrophage activation, were determined to reliably define lesion extent and correlate with neurobehavioral data, and justify invasive telemetered electromyographic and kinematic studies to more definitively address efficacy and mechanism.

Keywords

Spinal cord injury; African green monkey; Non-human primate; Stem cells; Biomaterials; Injury model; Behavioral scoring

1. Introduction

Spinal cord injury (SCI) results from penetrating or compressive traumatic injury to the spine or from compressive lesions associated with neoplastic growth or vertebral dislocation. Neuronal injury and recovery is critically guided and impacted by the surrounding cells and extracellular environment within the spinal cord and adjacent tissues, reducing the utility of *in vitro* assays, and necessitating the study of injury mechanisms and spinal cord physiology in *in vivo* vertebrate models (Feringa et al., 1975; Hall and Springer, 2004; Jones et al., 2005; Liverman et al., 2005; Thuret et al., 2006; Baptiste and Fehlings, 2007; Rossignol et al., 2007). A recent review of data derived from the extensive literature related to the modeling of SCI to better understand mechanisms of injury and repair has highlighted the greater relevance and utility of nonhuman primate models relative to rodents and other vertebrate species in the preclinical investigation of therapeutic interventions (Courtine et al., 2007). Rodents may over-predict the efficacy of interventions given high rates of spontaneous recovery from induced spinal cord injury, even following profound lesions. The spinal cord anatomy and physiology of old world monkeys are more similar to humans, particularly with respect to the position and function of corticospinal tracts (Courtine et al., 2007). This permits a more critical evaluation of results from preclinical studies, facilitating translation to humans. Here we report the development of a surgical model of acute SCI in the African green monkey (*Chlorocebus sabaeus*) for the evaluation of biomaterial implants as a translational interval between rodent and clinical investigations.

Poly(lactide-co-glycolide) (PLGA) biocompatible and biodegradable porous scaffolds seeded with neural stem cells (NSC) have demonstrated potential as a strategy for the treatment of central nervous system lesions (Flax et al., 1998; Park et al., 2002). A PLGA scaffold seeded with murine NSC (mNSC) promoted long-term functional improvements in an adult rat hemisection model of SCI as compared to controls (Teng et al., 2002). 70 days post-injury, treated animals exhibited coordinated, weight-bearing hindlimb stepping. Histological and immunocytochemical analysis suggested the recovery may have been associated with a reduction in tissue loss, possibly resulting from modulation of secondary injury mechanisms and reduced astrogliosis.

To establish an SCI model in which this possibility might be critically evaluated, a lateral hemisection at level T9–T10 in the thoracic spine was created in the monkey, with removal

of the ipsilateral T9–T10 segment. This approach bears some similarity to previously published models, where ipsilateral tracts were transected without removal of a full segment or only particular tracts (lateral corticospinal efferents, dorsal funiculus afferents) were targeted (Crowe et al., 1997; Babu et al., 2000; Edgerton et al., 2004). The lesion was designed to result in Brown-Séquard syndrome, characterized in humans at comparable cord levels by paralysis of the ispilateral leg, loss of ipsilateral muscle tone in the lower abdomen (innervated by T9–L1), loss of vibration and position sensation in the ipsilateral hindlimb, loss of thermal and mechanical pain sensation in the contralateral leg, lumbar and sacral dermatomes and ipsilateral lower thoracic dermatomes, and spastic paresis in the ipsilateral leg resulting in increased knee and ankle jerk reflexes with retention of monosynaptic reflexes involving the lower motor neurons (Brown-Séquard, 1851). Importantly, a unilateral restriction of the lesion was implemented with the additional aim of sparing bladder function and anal muscle tone by allowing compensatory innervation by retained contralateral corticospinal efferents. Evaluation of loss and recovery of these multiple lower extremity functions may permit objective measures of the efficacy of the therapeutic intervention with minimal post-operative complications.

In addition to establishing methodologies for the generation of a discrete unilateral cord lesion designed to minimize special animal care requirements, behavioral and histological endpoints were evaluated for their utility in differentiating treatment outcomes. Neuromotor and histopathological endpoints were assessed across multiple time points following introduction of a PLGA scaffold, PLGA scaffold seeded with hNSC, or no implant.

2. Materials and methods

2.1. Hemisection model

Four juvenile male African green monkeys ranging in weight from 2.3 to 2.7kg were employed in the study. Subjects were between 1.8 and 2.0 years old. Baseline clinical and neurological exams confirmed good health and suitability for study enrollment. Treatment allocation was performed arbitrarily with respect to weight. All experimental and surgical procedures were carried out in accordance with the Guide for the Care and Use of Laboratory Animals (National Academy Press, revised 1996) and the Institutional Animal Care and Use Committee (IACUC) of the St. Kitts Biomedical Research Foundation, where the study was conducted.

To perform the hemisection lesion, monkeys were sedated with ketamine/xylazine i.m., and kept on a 0.9% saline drip. Isoflourane anesthesia was applied with depth of anesthesia monitored throughout the study. Deep dermal or subcutaneous bleeding was controlled using electrocautery following skin incision. The laminectomy was performed by an en-bloc, lateral lamina cut method. Following bone removal, the dural opening was performed with a#15 surgicalblade. Dural edges were tacked to the surrounding ligaments or musculature with 4.0 nonabsorbable sutures. The midline of the spinal cord was carefully assessed with the visualization of anatomic landmarks. At all times, spinal cord veins and surface vessels were spared unless it was absolutely necessary that they be controlled. The segmental hemisection lesion was microscopically performed with the use of microneurosurgical dissection instruments and micro-suction aspiration. A transverse

incision extending to the midline was made at the caudal point of the intersection of the T9 dorsal root with the cord and at the rostral point of the intersection of the T10 dorsal root with the cord, followed by a midline incision extending between those levels. Hemi-cord parenchyma resection to these defined boundaries ensured complete transection to the anatomic midline in a lesion extending 10mm in length, without damage to the contralateral hemi-cord. At this point in the procedure, if designated, a scaffold was implanted (Fig. 1). The scaffold was sized to fill the hemisection cavity, without exerting pressure on the surrounding host tissue during or following insertion. When this process was complete, the dural tack-up sutures were removed, and the dura was closed with a 4.0 non-absorbable single running suture. Fibrin tissue sealant was applied to the dural suture line. The fascia was then closed with interrupted 3.0 absorbable sutures. After this layer was closed, the subcutaneous layers were re-approximated with 3.0 absorbable sutures. Then, the deep dermal layer was brought together with interrupted 3.0 absorbable sutures. After successful extubation and recovery from anesthesia, a neurologic examination was performed. Vital signs were monitored in a manner consistent with standard human post-anesthesia care. Following recovery from anesthesia the monkeys were returned to their cage with a mattress placed on the floor to minimize pressure sore risk. Monkeys were observed twice daily to assess skin integrity and exclude the possibility of autophagy, which can be observed in the setting of limb denervation. All monkeys additionally received a pre and postoperative course of immunosuppressants, consisting of cyclosporine (0.6 mg/kg), prednisolone (0.3 mg/kg) and azathioprine (0.5 mg/kg) i.m. BID starting 3 days before implantation and continuing until sacrifice to prevent hNSC rejection. Though this immunosuppressant regimen had been previously established to be well tolerated, additional attention and vigilance was maintained to prevent opportunistic infections.

2.2. Neuromotor video recordings

Video recordings of quadrupedal locomotion were generated for qualitative and quantitative assessment of gait and posture deficiencies associated with motor impairment of the ipsilateral hindlimb. To document locomotion, the monkeys were placed in an 8 × 2.5 × 2 foot ambulation chamber. One long side of the chamber was made of Plexiglas™ to allow visualization of the monkey as it navigated the enclosure. Movements were recorded by video continuously for a 4-min period with the entire width of the enclosure captured in the camera's field of view under optimized illumination. At the end of the 4-min video segment a food reward was introduced to the chamber through an aperture in the ceiling to promote and document upright standing, after which another 4 min of close-up video of the monkey was obtained. Video sessions were conducted prior to surgery, postoperative days 2,3, 4, 6 and 10 and then weekly for 6 weeks and prior to sacrifice.

Video data were reviewed and rated by a blinded reviewer not involved in the *in vivo* execution of the study. Ratings for each video session were based on review of the combined 4-min video segments collected during the wide field and close-up recordings. Ratings generated an overall observational neuromotor score for the ipsilateral and contralateral hindlimbs (Table 1). The rating scale incorporates the components derived from the spectrum of behaviors and motions observed in healthy African green monkeys and

was based on previously established methods for observational scoring (Basso et al., 1996; Babu et al, 2000).

2.3. Histology and immunohistochemistry

On the study day indicated in Table 2, the monkeys were euthanized with intravenous sodium pentobarbital followed by whole body perfusion fixation with 4% paraformaldehyde. Animals were examined carefully for external abnormalities including hair loss or decubitus ulcers at bony prominences, palpable masses, and abnormalities in the abdominal, thoracic, and cranial cavities. The sciatic nerves, spinal cord and brain were dissected en masse and fixed overnight in 4% paraformaldehyde, following which specimens were transferred to phosphate buffered saline.

The fixed tissue was treated overnight with 20% glycerol and 2% dimethylsulfoxide and embedded in a gelatin matrix using MultiBrain™ (NeuroScience Associates, Knoxville, TN). After curing in weak formaldehyde solution, the block was rapidly frozen by immersion in 2-methyl butane chilled to −70 °C with crushed dry ice and mounted on an A860 sliding microtome. The block was sectioned to generate alternating 40 μm sagittal and coronal sections spanning the lesion site as well as cervical, thoracic and lumbar regions rostral and caudal to the lesion. For each stain, every 24th section at 720 μm intervals was mounted and processed, yielding approximately 20 individual sections mounted on 10 slides. For ionized calcium-binding adapter molecule (Iba1) staining, sections were stained free-floating. Sections were treated with hydrogen peroxide and blocking serum, and immunostained with a 1:15,000 dilution of primary polyclonal rabbit anti-Iba1 antibody (#01973, WAKO, http://wakousa.com), a goat anti-rabbit secondary antibody, and an avidin-biotin-HRP complex (Vectastain ABC kit, Vector, Burlingame, CA). Incubation times were 24h (4°C) for the primary antibody, 30 min (room temperature) for the secondary antibody, and 1h (room temperature) for the avidin–biotin–HRP complex. Sections were subsequently treated with diaminobenzidine tetrahydrochloride (DAB) and mounted on gelatinized (subbed) glass slides. Amino cupric silver staining was performed as described previously (De Olmos et al., 1994).

Adobe Photoshop Creative Suite 4 Extended was used for cord image compilation and analysis. For each cord, the original 8–10 microscopic images of the sections containing the lesions were consolidated using *Photomerge* in the *reposition* layout, shown in Fig. 9. Guidelines for cord lengths and widths were formulated using the straight line tool, and their pixel measurements were taken using *Ruler tool*. For lesion areas, original cord border was approximated with the outline of the spared portion as a reference with the help of the *magnetic lasso* under 10% contrast settings and the *brush.* Area measurements with square pixel units were taken using the *magnetic lasso and record measurements with area data points*.

Due to the curvature of both X992 and Y156, the cord images were straightened out to obtain more realistic data for quantification of lesion dimensions. While keeping cord width constant between the original and modified images, *warp* was used to straighten out the image and prepare it for measurements.

All data was converted from pixel units to metric units using measurements recorded from the original cord samples. Cord widths were then normalized to 6 mm for all samples, to enable comparison and remove histological artifact. Linear and area dimensions were adjusted accordingly and summarized in Table 3.

2.4. Poly(lactide-co-glycolide) implants

Poly(lactide-co-glycolide) (PLGA) polymer porous scaffolds were prepared in a similar manner to previously published protocols (Mikos et al., 1992; Lavik et al., 2002; Teng et al., 2002). The implant was sized to precisely fit the spinal cord cavity, created by the segmental hemisection surgical resection. The size of the lesion was determined prior to live surgery by measurement of the spinal cord of a cadaver African green monkey, of similar weight to the enrolled subjects. The ratio of lactic to glycolic acid units in the PLGA was chosen in order for the scaffold to degrade over a period of 4–8 weeks *in vivo* (Sung et al., 2004). PLGA with a lactide/glycolide ratio of 50:50 and intrinsic viscosity 0.55–0.75 dL/g was obtained from Lactel (Durect, Pelham, AL). Thin polymer foams were fabricated by solvent casting/particulate leaching. PLGA was dissolved in chloroform (Sigma, St. Louis, MO) to obtain a 5%w/v stock solution. The stock solution was mixed with sodium chloride (particle size 180–450 μm by sieving; Sigma) in a 1:1.67 ratio (3 mL/5 g) and poured into a 5.5 cm diameter Teflon™ mold. After chloroform was evaporated in a fume hood for 48 h, the salt particles were leached out by immersion in distilled water for 48 h at room temperature. The water was changed every 4–8 h during the leaching period. Subsequently, PLGA foam disks were dried on blotting paper and lyophilized overnight to remove residual water. The process yielded highly porous foam with a thickness of 1 mm. The foams were cut into segments (5 cm × 2 cm) with a surgical razor blade (VWR, West Chester, PA) and stored in 50 mL polypropylene Falcon test tubes (BD Biosciences, San Jose, CA) in a secondary container over anhydrous calcium sulfate (Drierite, Xenia, OH) at −20°C until use.

2.5. Cell seeding on poly(lactide-co-glyolide) scaffolds

Scaffolds were trimmed to 5 mm × 12 mm × 1 mm, prior to seeding. As PLGA is hydrophobic, the scaffolds were immersed in 70% ethanol for 30 min on an orbital shaker at room temperature (Daigger, Vernon Hills, IL), for the purpose of removing air inside the pores, sterilizing the accessible surface for cell attachment, and pre-wetting the scaffolds prior to immersion in aqueous media (Mikos et al., 1992). The excess ethanol was then removed and the scaffolds were washed 3 times for 10 min in sterile phosphate buffered saline (PBS, pH 7.4, Invitrogen, Carlsbad, CA) solutions and transferred individually to sterile 2 mL Eppendorf™ centrifuge tubes (Daigger) containing 1.5 mL sterile PBS solutions with extracellular matrix (ECM) adhesion molecules (10μg/mL): poly-D-lysine (Sigma, St. Louis, MO), laminin (BD Biosciences, San Jose, CA), and fibronectin (Sigma, St. Louis, MO). Scaffolds were left overnight on a sterilized orbital shaker platform to ensure sufficient adsorption of the adhesion proteins on the accessible scaffold surface, as well as full hydration inside the scaffold pores. The following day, supernatant was removed, and the scaffolds were transferred to a 6 well culture plate (Falcon™, BD Biosciences, San Jose, CA), followed by two 5 min rinses in fresh Neurobasal™ medium (with B27-A supplement, Invitrogen, Carlsbad, CA) on an orbital shaker (45 rpm).

Human neural stem cells (hNSC, clone HFB2050) were maintained in Falcon™ culture flasks in modified Neurobasal™ cell culture medium (with B27 supplements, antibiotics, heparin, and L-glutamine) in a humid incubator (37°C, 5%CO_2) (Flax et al., 1998). Prior to seeding, cells were lifted from the flasks using Accutase™ (Innovative Cell Technologies, San Diego, CA), and concentrated to 5×10^5 per mL to 1×10^6 per mL via a series of centrifugation, cell counting, and re-suspension in fresh medium. The first time the scaffolds were seeded with hNSC is considered an acclimation seeding. For the acclimation seeding, 2 mL of 5×10^5 per mL hNSC were used in each well in a 6 well plate. The plates were gently rotated in a sterilized humid chamber on an orbital shaker at 37°C for 30 min (40 rpm). For subsequent cell seedings, 2 mL of 1×10^6 per mL hNSC were used. Following the rotations, 3 mL of fresh modified Neurobasal™ medium were added to each well, and growth factors (20 ng/mL, basic fibroblast growth factor, bFGF, Cal-biochem, San Diego, CA; 10 ng/mL, leukemia inhibitory factor, LIF, Chemicon, Temecula, CA; 20 ng/mL, epidermal growth factor, EGF, Invitrogen, Carlsbad, CA), and the plates were maintained in the incubator. The plates were observed under sterilized light microscope twice daily, and 2.5 mL of the 5 mL total culture medium in each well was replaced with fresh medium and new growth factors every 3 days. The seedings were repeated at total of 4 times (including the acclimation seeding) with an average interval of 1 week in between each seeding. Films of PLGA approximately 200 μm thick were sterilized in 70% ethanol and maintained in serum containing medium for 1 week.

At the end of the scaffold seeding period, light-field microscopy was carried out on scaffolds in the culture plates, and images of attached hNSC inside the scaffold pores were captured using an AxioCam™ MRc on an AxioVert™ S100 inverted microscope (Carl Zeiss Microimaging, Thornwood, NY). Representative scaffolds were then fixed in 4% paraformaldehyde at 4°C overnight (on the same day as the surgeries were carried out using scaffolds from the same seeding wells), cryoprotected in 30% sucrose solution, embedded in OCT™ compound (Sakura Finetek, Torrance, CA), and cut into 20 μm thick serial sections for immunocytochemical (ICC) analysis. The scaffolds were oriented in the embedding compound in such a way that the sections are across the width (5 mm side) of the scaffold.

Microslides with scaffold sections were coverslipped with Fluorescent Mounting Medium with DAPI (Vector Labs, Burlingame, CA), and fluorescent images were captured via an AxioCam™ MRm on an AxioVert™ S100 inverted microscope (Carl Zeiss Microimaging) with a DAPI-specific color filter. Montage images of the entire cross-section were created from multiple shots at 10× magnification, which show clear identification of the nucleus of each attached hNSC. Occasionally, higher magnification images were captured in areas where too many cells cluster. The images were then printed inverted with high resolution so that each nucleus appears as a black dot. The total numbers of nuclei stained in each cross-section were counted, and sections from the ends and the center of the scaffolds were used for this practice. The average cell numbers (n) in each cross-section (20 μm) were used to estimate the total number (N) of hNSC seeded in each scaffold ($N = n \times$ (scaffold length/20 μm)). The cell nucleus counting follows the principle of conservative counting, by which only the clearly distinguishable nuclei were counted. Given the fact that some cells are washed off during the staining process, and some nuclei were not visible if they were behind

others, the total *N* estimates derived from this counting method represent a somewhat deflated version of the true cell numbers.

3. Results

3.1. Implants

The implant was designed as a porous PLGA scaffold to support seeded hNSC and permit in-growth of endogenous cells *in vivo*, as well as facilitating nutrient and waste transport. The pores were approximately 300 μm in diameter (Fig. 2). To facilitate cell seeding, cells were seeded on scaffold layers, 1 mm in thickness, which were subsequently sutured together with an outer layer to yield a three-dimensional hemi-cylindrical structure (Fig. 3). The outer layer of the implant was designed to emulate the spinal cord dura, to inhibit infiltration of meningeal cells into the scaffold in case the dura was not completely resealed post-surgery. The outer layer consisted of a solid PLGA sheet, approximately 200 μm in thickness.

The seeding protocol led to scaffolds with hNSC attached to the outer surface, as well as the inner walls of the pores inside the scaffolds (Fig. 4). Based on 6 sections from 2 scaffolds, the average number of hNSC attached in each 20 μm scaffold section $n = 4922$, which translates to approximately 2.5 million hNSC in a 10 mm × 5mm × 1 mm scaffold. Therefore, there were an estimated 5 million hNSC on assembled scaffolds.

3.2. Neuromotor outcomes

Monkeys were enrolled in the study according to the treatment schedule indicated in Table 2. The spinal cord hemisection procedure and placement of the scaffold or scaffold seeded with hNSC (scaffold + hNSC) was well tolerated in all subjects. Throughout the duration of the study the monkeys remained in good health. The T9–T10 hemisection resulted in Brown-Séquard syndrome with paralysis of the ispilateral leg, slight reduction in ipsilateral muscle tone in the lower abdomen, loss of pain sensation in the contralateral leg, and spastic paresis in the ipsilateral leg with increased knee and ankle jerk reflexes. There was a preservation of bladder and bowel tone, including in the acute setting, and no evidence of joint contractures in the paretic limb. Induced neuromotor deficits were observed in the immediate post-operative setting. One monkey (Y430) developed a sore on the dorsal surface of the ipsilateral (left) foot 2 weeks post-injury, as a result of loss of dorsiflexion. The wound improved with routine wound care.

Video recordings of quadrupedal locomotion and object retrieval in the ambulation chamber permitted an assessment of gait and posture deficits and improvements over time. Application by a trained observer of the specified video scoring procedure (Table 1) to recorded video segments provided a reproducible measure of leg, foot and toe positioning and movements, postural changes and overall neuromotor changes. Changes in the video based neuromotor score were defined for the in the ipsilateral (left) and contralateral (right) side of each monkey (Fig. 5).

3.3. Histopathology and immunohistochemistry

Hematoxylin and eosin (H&E) stained cross-sections in the thoracic region rostral and caudal to the injury center were examined, showing clear anatomic evidence for the observed Brown-Séquard syndrome in all subjects. In rostral sections, there was severe degeneration of ipsilateral dorsal funiculus afferent tracts, as confirmed by the presence of swollen axons, necrosis and lymphocyte and macrophage invasion. Severe ipsilateral degeneration of lateral and ventral corticospinal tract efferents was also observed. In caudal sections, there was bilateral preservation of dorsal funiculi afferents. The degree of lymphocyte recruitment to afferent and efferent tracts, rostral and caudal to the injury site respectively, varied between subjects.

H&E staining revealed small amounts persisting polymer debris in the scaffold + hNSC subject sacrificed at 40 days post-injury (Fig. 6(A) and (B)). There was minimal evidence of persisting polymer in the scaffold + hNSC sacrificed at 82 days post-injury, suggesting complete degradation and clearance of the scaffold within this time frame in vivo (Fig. 6(C) and (D)).

H&E staining revealed evidence of fibrous matter around the lesion in two subjects, namely the scaffold treated subject sacrificed at 83 days post-injury (Y464) and the scaffold + hNSC treated subject sacrificed at 82 days post-injury (Y430). This was observed as birefringence using a polarizing filter under an optical microscope, often an indication of collagen deposition. It is possible that, in these subjects, the resealed dura did not remain completely intact following surgery, permitting infiltration of fibroblasts into the injury site. As the influx of meningeal cells could play a significant role in the pathological profile of the lesion, the consistency of dural integrity is important across subjects in the development of a central nervous system injury model.

H&E staining also revealed lines of hemocynanin deposition, demarking severed blood vessels within the spinal cord. Blood flowing under pressure from severed blood vessels, in particular arterial vessels, is a possible source of mechanical insult to nervous system tissue surrounding the lesion. In addition, damaged blood vessels result in local ischemia. The presence of multinucleated giant cells around the lesion site was observed in all subjects, and it is unclear to what extent, if at all, these were specifically present in response to foreign polymer materials and allogeneic hNSC.

Silver degenerative staining of cross-sections rostral and caudal to the lesion provided an indication of the extent of axonal disruption. The lesions remained unilateral in the lateral regions, with severe degeneration of ipsilateral lateral corticospinal tract (CST) efferents (Fig. 7). Some degree of variability between subjects exists at the midline in dorsal funiculus afferents (Fig. 8 (A), (C), (E) and (G)). In all animals, longitudinal sections through the lesion site showed clear evidence that, at the time of analysis, the lesion had crossed the cord midline, resulting in loss of grey matter on the contralateral side (Fig. 9), further studied by quantification of lesion dimensions (Table 3). Axonal damage was observed both ipsilaterally and contralaterally in ventral–medial tracts (Fig. 10). The small sample size, however, was not intended to distinguish the degree to which these differences were due to variations in the surgical lesion and individual responses to trauma compared to secondary

injury and wound healing processes that may hypothetically be influenced by implantation of scaffolds and hNSC (Teng et al., 2002).

Iba1 immunohistochemistry provided an indication of reactive microglial and macrophage abundance and distribution, providing a further measure of the degree to which the impact of the hemisection remained unilateral weeks post-injury. The lesions remained unilateral in the lateral regions, with substantial Iba1 immunoreactivity around ipsilateral lateral CST efferents (Fig. 11). A similar degree of variability as observed by silver staining was observed using Iba1 immunohistochemistry in the dorsal funiculus rostral to the injury site (Fig. 8(B), (D), (F) and (H)).

4. Discussion

Creation of a hemisection in the thoracic spine at the T9–T10 level in the African green monkey resulted in paralysis of the ipsilateral hindlimb, with concomitant sparing of bladder and rectal function and retention of sufficient overall motor function and mobility and allowed the continuation of feeding, grooming and other healthy activities without supplementary veterinary care. Behavioral evaluations confirmed improvement in post-operative paralysis over time, but improvement was gradual with sufficient remaining deficit to allow definition of recovery rate and distinction within subjects between phases of recovery and between subjects exhibiting different degrees of impairment. As such, this African green model of SCI may represent a means by which the safety and efficacy of therapeutic SCI interventions in a clinically relevant species could be assessed humanely.

This study was primarily designed to evaluate the feasibility of implementing a lateral hemisection model of SCI in a non-human primate, and to identify the specific clinically relevant behavioral and pathological endpoints that could be reproducibly obtained. Coupled kinematic and electromyographic measures in previous primate studies have demonstrated the feasibility of obtaining these critical endpoints (Courtine et al., 2005). The associated telemetry and surgical interventions, however, are, in themselves, a significant research investment and variable impacting animal wellbeing, with the established need for prolonged postoperative care. The more critical question addressed in this study was the consequence and tolerance of a T9–T10 hemisection lesion, and a characterization of the overall neuromotor phenotype and its evolution over time such that more definitive efficacy and mechanism studies could be rationally and humanely designed. Therefore, the sizes of the treatment groups in the present study were limited and not designed to provide statistical evaluation of the the rapeutic efficacy of the implanted PLGA scaffold or PLGA scaffold seeded with hNSC at the lesion site. All subjects exhibited a return toward baseline neuromotor scores in the ipsilateral hindlimb, which exhibited complete post-operative paralysis following the T9–T10 lesion. This indicates a degree of recovery and neural plasticity consistent with reported findings in other primate SCI models (Edgerton et al., 2004). This observation encourages additional application of the model for more definitive preclinical studies in a larger study cohort to evaluate the therapeutic efficacy of PLGA scaffolds and human neural stem cells in the promotion of SCI recovery and repair.

Video capture of neuromotor behavior in the ambulation chamber provided a means of documenting and scoring neuromotor deficits and improvement over time. An observation based scoring system, however, may be inadequate to give precise information of neuromotor performance, due to the potential for the contralateral side to compensate for any loss of weight bearing ability and posture resulting from a unilateral interruption of motor and sensory pathways to the injured hindlimb. The application of kinematics, electromyography and evoked potentials would contribute to improved measures of neurologic function and quantification of ipsilateral and contralateral deficit and recovery (Courtine et al., 2009).

Histological analysis confirmed creation of a thoracic lesion in all study monkeys. Hematoxylin and eosin staining provided a definition of the extent of the lesion and degree of injury associated lymphocyte invasion, axonal swelling and macrophage infiltration, as well as a circumscribed degree of hemorrhage and gross necrosis. Silver staining revealed clear degenerative changes consistent with interruption of ipsilateral efferent lateral corticospinal tracts at the thoracic level caudal to the lesion and sensory afferents rostral to the lesion. It was noted that the ventral–medial region of the cord, which contains both important sensory and motor tracts, may be particularly sensitive to different degrees of bilateral surgical injury among subjects. Iba1 immunohistochemistry exhibited a distribution that paralleled the degenerative findings highlighted by the silver staining. As such, Iba1 constituted an additional measure of the degree of injury and repair.

Histological evaluations confirmed the creation of a lesion with severe degeneration of ipsilateral motor and sensory axons. In no animals were the degenerative changes entirely unilateral. While contralateral corticospinal tracts were extensively preserved in all subjects, in addition to the majority of the dorsal horn in most subjects, contralateral damage was observed in the ventral–medial region in all subjects. Contralateral damage is most due to surgical variability, which will be improved in future, more sophisticated, investigations.

The persistence of the PLGA scaffold for at least 40 days, and degradation and clearance from the spinal cord within 82 days post-implantation was observed. Two important changes were made to the neural stem cells seeded PLGA scaffold used in this study, in comparison with a similar rodent study (Teng et al., 2002). Firstly, human neural stem cells (hNSC) were used instead of murine neural stem cells. Secondly, the PLGA scaffold was redesigned in response to observations made in the rodent study (Teng et al., 2002).The relative volume of the inner scaffold was increased to accommodate more hNSC. It was postulated that a major mechanism of action of the implanted cells may be due to trophic support rather than neuronal replacement (Yu et al., 2009). Therefore, it was hypothesized that a larger number of hNSC could increase any therapeutic effect. It was also proposed that the ‘outer scaffold’ in the rodent study, consisting of longitudinally oriented channels intended to permit axon in-growth, may have also served to prevent meningeal inflammatory cell infiltration. Unpublished *in vitro* data showed that the channels were impermeable to fibroblasts. To maximize the size of the inner scaffold, while providing a physical barrier to meningeal cell infiltration, the outer scaffold was constructed as a 200 μm thin, flexible sheet of PLGA. The observed tolerance of the current implant will guide implant design for further studies.

The ability to model spinal cord injury by lateral, segmental hemisection in African green monkeys with limited impact on overall wellbeing presents a useful model for the assessment of spinal cord injury repair and response to intervention. Greater sensitivity and specificity to treatment effects could be achieved through expanded samples sizes to address lesion variability and application of coupled kinematic and electromyographic analyses, as well as further histological markers to identify specific mechanisms involved in secondary injury, repair and regeneration.

Supplementary Material

Refer to Web version on PubMed Central for supplementary material.

Acknowledgments

Human neural stem cells generated and provided by Evan Y. Snyder (Burnham Institute for Medical Research, La Jolla, CA, esnyder@burnham.org). We thank William L. Neeley for assistance with PLGA scaffold fabrication (MIT, Cambridge, MA), Darcy Benedict for assistance with cell culture and seeding (Brigham and Women's Hospital, Boston, MA) and Dr. D. Eugene Redmond Jr. for assistance with surgical procedures and animal care (St. Kitts Biomedical Research Foundation, St. Kitts and Nevis). We thank Robert C. Switzer III for assistance with staining protocols (NeuroScience Associates, Knoxville, TN). We thank George Calapai for video editing, Lauren Mitarotondo for writing assistance and Janice Ye for image analysis (InVivo Therapeutics, Cambridge, MA). C.D.P. was supported by the MIT/CIMIT Medical Engineering Fellowship. InVivo Therapeutics thanks its investors and advisors for support. This study was funded by InVivo Therapeutics Corporation.

References

Babu RS, Muthusamy R, Namasivayam A. Behavioural assessment of functional recovery after spinal cord hemisection in the bonnet monkey. Journal of Neurological Sciences. 2000; 178:136–52.

Baptiste DC, Fehlings MG. Update on the treatment of spinal cord injury. Progress in Brain Research. 2007; 161:217–33. [PubMed: 17618980]

Basso DM, Beattie MS, Bresnahan JC. Graded histological and locomotor outcomes after spinal cord contusion using the NYU weight-drop device versus transaction. Experimental Neurology. 1996; 139:244–56. [PubMed: 8654527]

Brown-Séquard CÉ. De la transmission croisée des impressions sensitives par la moelle épinière. Comptes rendus de la Société de biologie. 1851; 2:33–44.

Courtine G, Roy RR, Hodgson J, McKay H, Raven J, Zhong H, Yang H, Tuszynski MH, Edgerton VR. Kinematic and EMG determinants in quadrupedal locomotion of non-human primate (rhesus). Journal of Neurophysiology. 2005; 93:3127–45. [PubMed: 15647397]

Courtine G, Bartlett Bunge M, Fawcett JW, et al. Can experiments in nonhuman primates expedite the translation of treatments for spinal cord injury in humans? Nature Medicine. 2007; 13(5):561–6.

Courtine G, Gerasimenko Y, van den Brand R, Yew A, Musienko P, Zhong H, Song B, Ao Y, Ichiyama RM, Lavrov I, Roy RR, Sofroniew MV, Edgerton VR. Transformation of nonfunctional spinal circuits into functional states after the loss of brain input. Nature Neuroscience. 2009; 12:1333–42.

Crowe MJ, Bresnahan JC, Shuman SL, Masters JN, Beattie MS. Apoptosis and delayed degeneration after spinal cord injury in rats and monkeys. Nature Medicine. 1997; 3(1):73–6.

De Olmos JS, et al. Neurotoxicology and Teratology. 1994; 16:545–61. [PubMed: 7532272]

Edgerton VR, Tillakaratne NJK, Bigbee AJ, de Leon RD, Roy RR. Plasticity of the spinal neural circuitry after injury. Annual Review of Neuroscience. 2004; 27:145–67.

Feringa ER, Johnson RD, Wendt JS. Spinal cord regeneration in rats after immuno-suppressive treatment. Theoretic considerations and histologic results. Archives of Neurology. 1975; 32(10): 676–83.

Flax JD, Aurora S, Yang C, et al. Engraftable human neural stem cells respond to developmental cues, replace neurons, and express foreign genes. Nature Biotechnology. 1998; 16:1033–9.

Hall ED, Springer JE. Neuroprotection and acute spinal cord injury: a reappraisal. NeuroRx. 2004; 1:80–100. [PubMed: 15717009]

Jones TB, McDaniel EE, Popovich PG. Inflammatory-mediated injury and repair in the traumatically injured spinal cord. Current Pharmaceutical Design. 2005; 11:1223–36. [PubMed: 15853679]

Lavik E, Teng YD, Snyder E, Langer R. Seeding neural stem cells on scaffolds of PGA, PLA, and their copolymers. Methods in Molecular Biology. 2002; 198:89–97. [PubMed: 11951644]

Liverman, CT.; Altevogt, BM., et al. Spinal cord injury: progress, promises and priorities. Washington, DC: National Academies Press; 2005.

Mikos AG, Sarakinos G, Leite SM, Vacanti JP, Langer R. Laminated three-dimensional biodegradable foams for use in tissue engineering. Biomaterials. 1992; 14(5):323–30. [PubMed: 8507774]

Park KI, Teng YD, Snyder EY. The injured brain interacts reciprocally with neural stem cells supported by scaffolds to reconstitute lost tissue. Nature Biotechnology. 2002; 20:1111–7.

Rossignol S, Schwab M, Schwartz M, Fehlings MG. Spinal cord injury: time to move? The Journal of Neuroscience. 2007; 27(44):11782–92. [PubMed: 17978014]

Sung HJ, Meredith C, Johnson C, Galis ZS. The effect of scaffold degradation rate on three-dimensional cell growth and angiogenesis. Biomaterials. 2004; 25:5735–42. [PubMed: 15147819]

Teng YD, Lavik EB, Qu X, Park KI, Ourednik J, Zurakowski D, Langer R, Snyder EY. Functional recovery following traumatic spinal cord injury mediated by a unique polymer scaffold seeded with neural stem cells. Proceedings of the National Academy of Sciences of the United States of America. 2002; 99(5):3024–9. [PubMed: 11867737]

Thuret S, Moon LDF, Gage FH. Therapeutic interventions after spinal cord injury. Nature Neuroscience. 2006; 7:628–43.

Yu D, Neeley WL, Prichard CD, Slotkin JR, Woodard EJ, Langer R, Teng YT. Blockade of peroxynitrite-induced neural stem cell death in the acutely injured spinal cord by drug-releasing polymer. Stem Cells. 2009; 27:1212–22. [PubMed: 19418456]

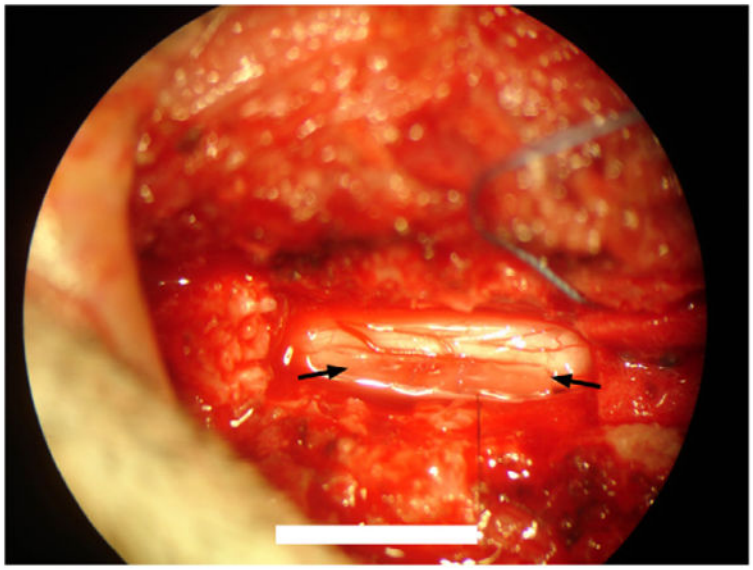

Fig. 1.

Photograph through surgical microscope of scaffold implanted into T9–T10 hemisection lesion. Arrows indicates scaffold position. Scale bar = 10mm.

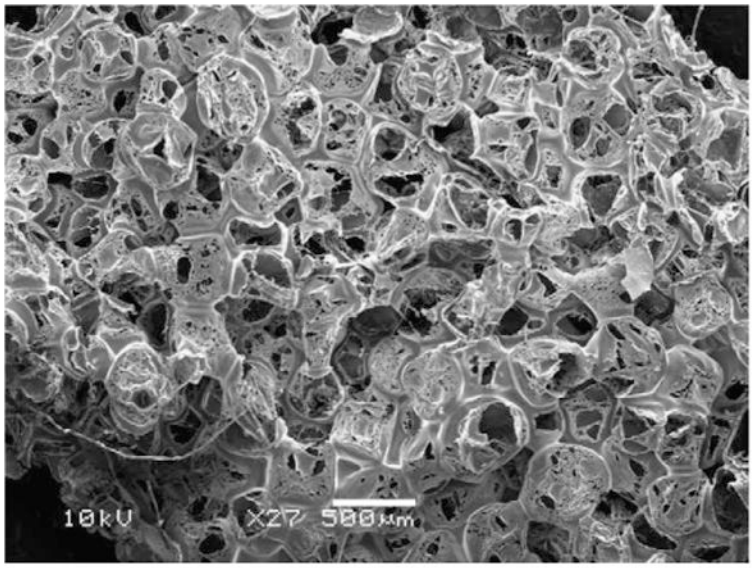

Fig. 2.
Scanning electron microscope image of scaffold architecture.

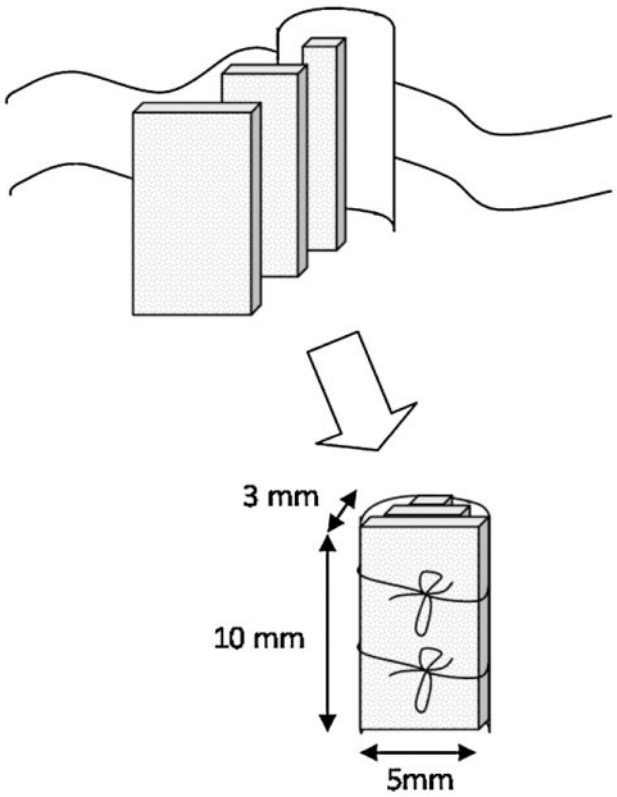

Fig. 3.
Composite scaffold design.

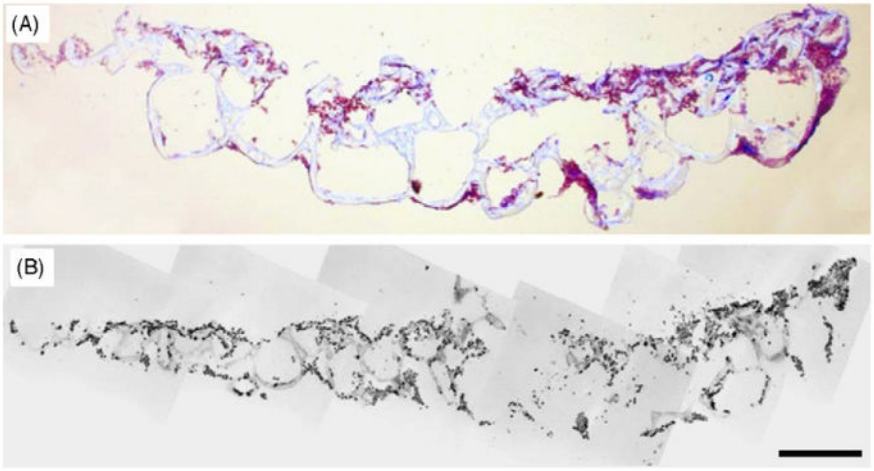

Fig. 4.

Seeding of hNSC on PLGA scaffolds. (A): Microscope image of toluidine blue staining of a cross-section of a PLGA scaffold seeded with hNSCs (purple dots). (B): Montage of multiple microscope images of the different areas of the same scaffold cross-section; inverted greyscale image of DAPI fluorescence (black dots are hNSC nuclei stained for DAPI). Scale bar = 500 μm. (For interpretation of the references to color in this figure legend, the reader is referred to the web version of the article.)

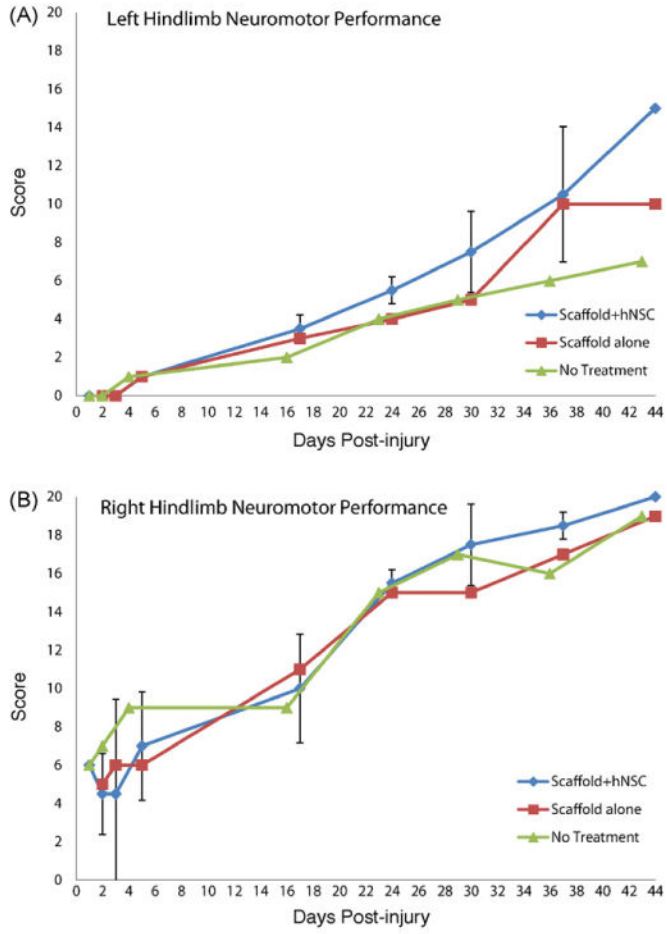

Fig. 5.

Temporal profile of functional recovery post-injury. (A): Video neuromotor scores in ipsilateral (left) hindlimb. (B): Video neuromotor scores in contralateral (right) hindlimb. Designations are as follows: Scaffold + hNSC: mean and standard deviation for Y430 and X992; $n = 2$ except for day 1 and day 44 where $n = 1$ due to sacrifice of X992 at 40 days post-injury. Scaffold alone: Y464. Control (no treatment): Y156.

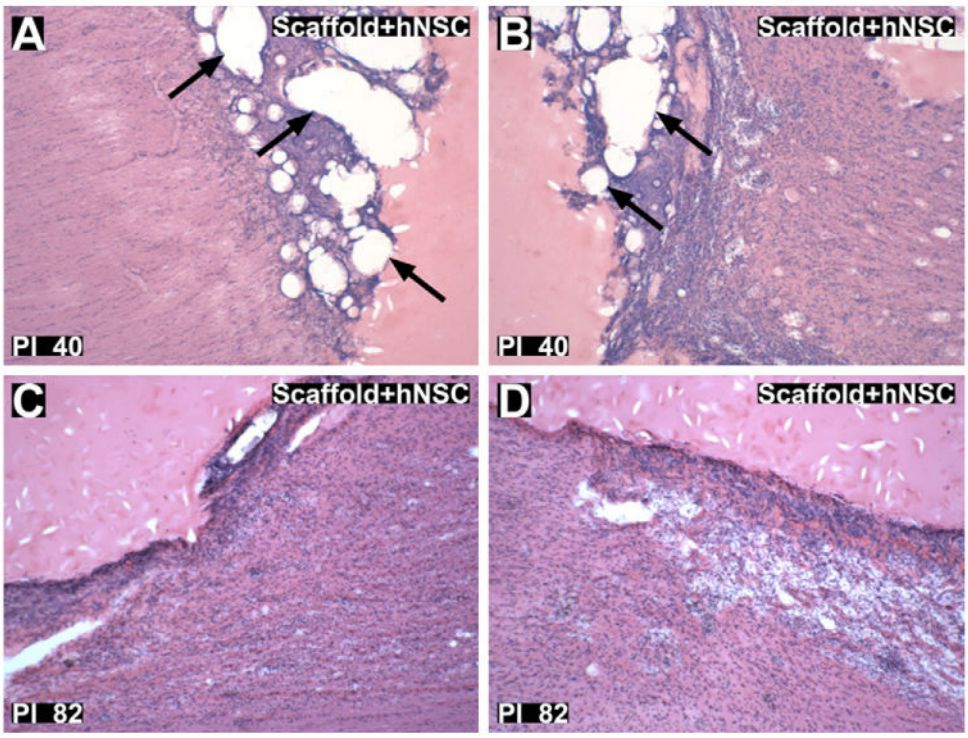

Fig. 6.

Hematoxylin and eosin staining of lesion margins. (A and B): Rostral (A) and caudal (B) lesion margins of scaffold + hNSC treated animal 40 days post-injury (X992). Arrows indicate preserved polymer matrix. (C and D): Rostral (C) and caudal (D) lesion margins of scaffold + hNSC treated animal 82 days post-injury (Y430). There was no appreciated polymer matrix, indicating substantial degradation and clearance of the scaffold within 82 days in vivo. Glial cell proliferation and mononuclear cell infiltration adjacent to the lesion margin is visible in both subjects (A and D). Magnification = 40×.

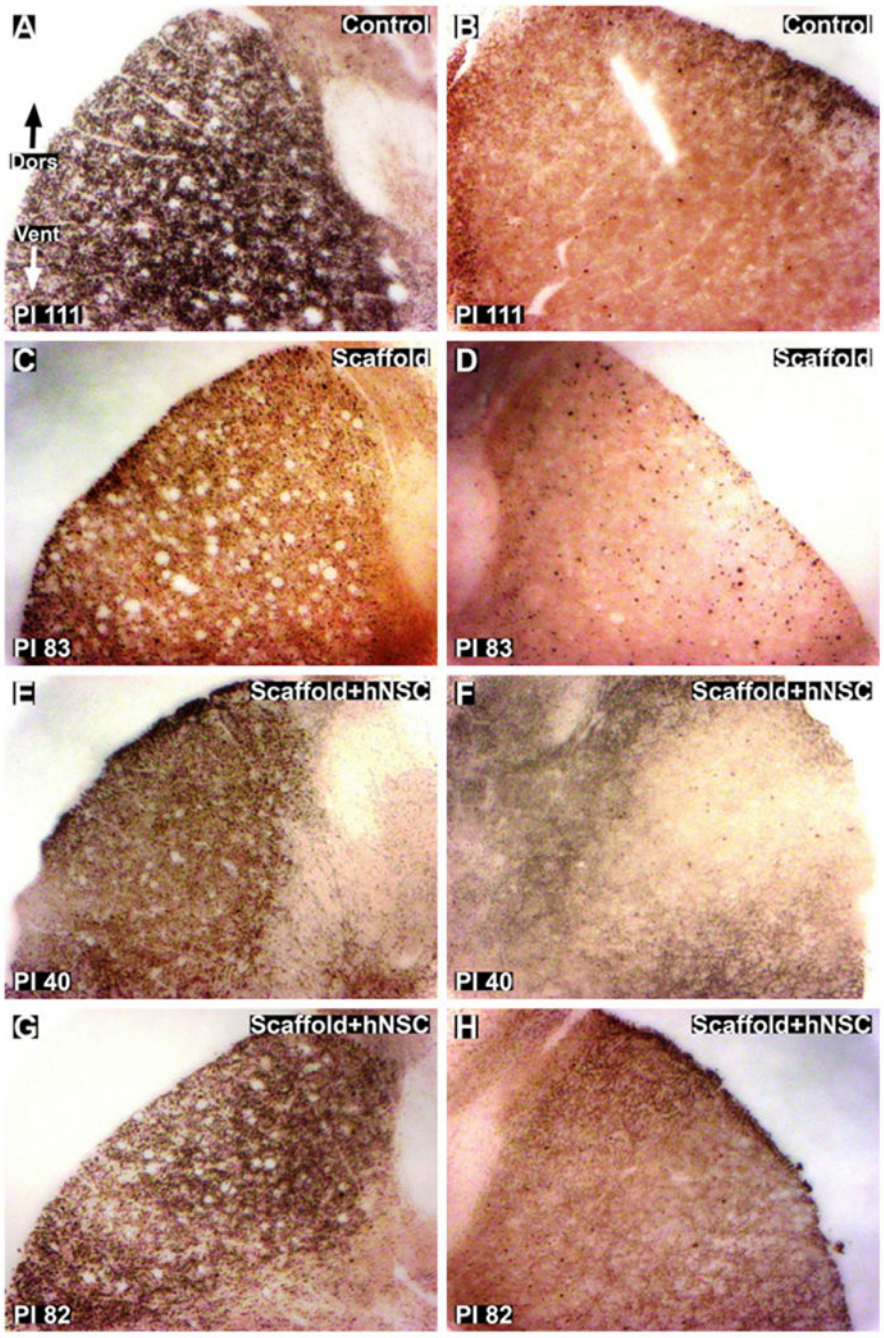

Fig. 7.

Silver staining for axonal degeneration of lateral corticospinal tracts (CST) in thoracic cross-sections caudal to the injury site. (A and B): Ipsilateral (A) and contralateral (B) images of control subject 111 days post-injury. C and D: ipsilateral (C) and contralateral (D) images of scaffold treated subject 83 days post-injury. E and H: Ipsilateral (E and G) and contralateral (F and H) images of scaffold + hNSC treated subjects 40 (E and F) and 82 (G and H) days post-injury. The lesion is unilateral with respect to degeneration of axons in the CST. Dors = dorsal. Vent = ventral. Magnification = 10×.

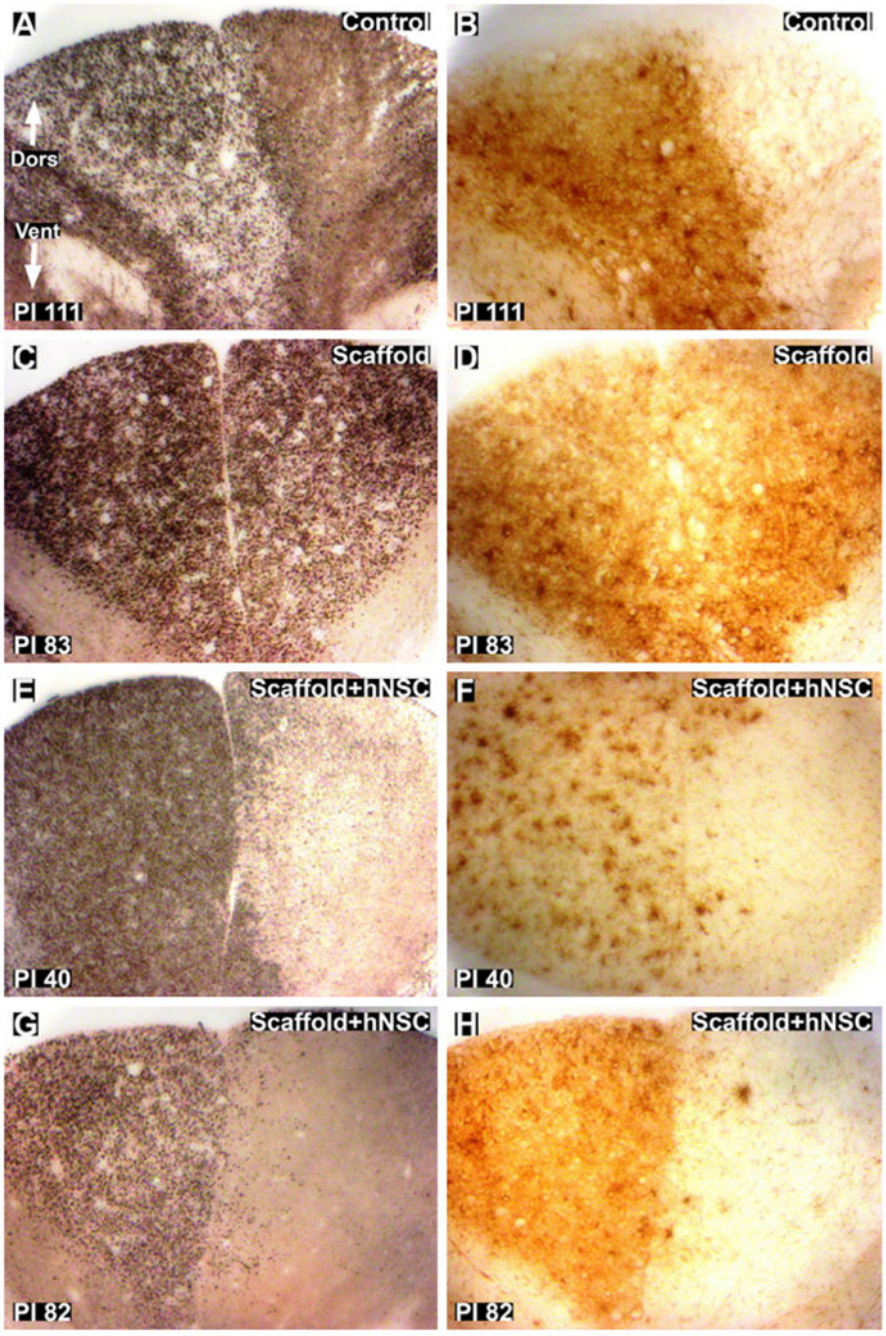

Fig. 8.

Silver staining and Iba1 staining of the dorsal funiculus in thoracic cross-sections rostral to the injury site. (A and B): Silver (A) and Iba1 (B) staining of control subject 111 days post-injury. The lesion crosses the midline slightly in the control subject in the dorsal funiculus. (C and D): silver (C) and Iba1 (D) staining of scaffold treated subject 83 days post-injury. The images show total bilateral damage to the dorsal funiculus in the scaffold treated subject. E and H: silver (E and G) and Iba1 (F and H) staining of scaffold + hNSC treated subjects 40 (E and F) and 82 (G and H) days post-injury. The lesion is predominately

unilateral, with some axonal degeneration of contralateral dorsal funiculus afferents with spatially correlating microglial and macrophage activation. Dors = dorsal. Vent = ventral. Magnification = 10×.

Fig. 9.

Silver staining for axonal degeneration in thoracic sagittal sections through the hemisection lesions. Sections shown are closest to the middle of the cord in the rostral–caudal direction. (A): Control subject 111 days post-injury. B: scaffold treated subject 83 days post-injury. (C and D): Scaffold + hNSC treated subjects 40 (C) and 82 (D) days post-injury. The lesion crosses the midline, in reference to the central canal where present, into the contralateral gray matter. In these sections the contralateral lateral funiculi appear to be preserved from the surgical lesion in all subjects. However, some degenerative staining is visible in contralateral efferents. Ipsi = ipsilateral lesioned side. Contra = contralateral unlesioned side. The cords are oriented rostral to caudal from left to right. Scale bar = 1mm.

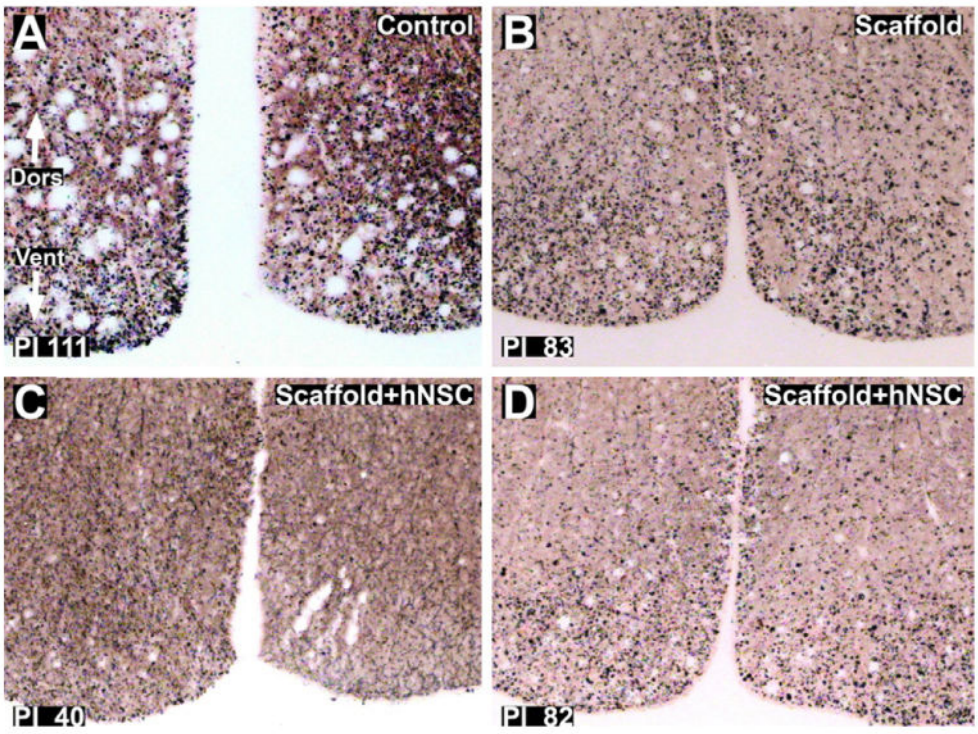

Fig. 10.

Silver staining for axonal degeneration of ventral funiculus tracts in thoracic cross-sections caudal to the injury site. (A): Control subject 111 days post-injury. B: scaffold treated subject 83 days post-injury. C and D: scaffold + hNSC treated subjects 40 (C) and 82 (D) days post-injury. The lesion is bilateral with respect to degeneration of axons in the ventral–medial tracts. Dors = dorsal. Vent = ventral. Magnification = 10×.

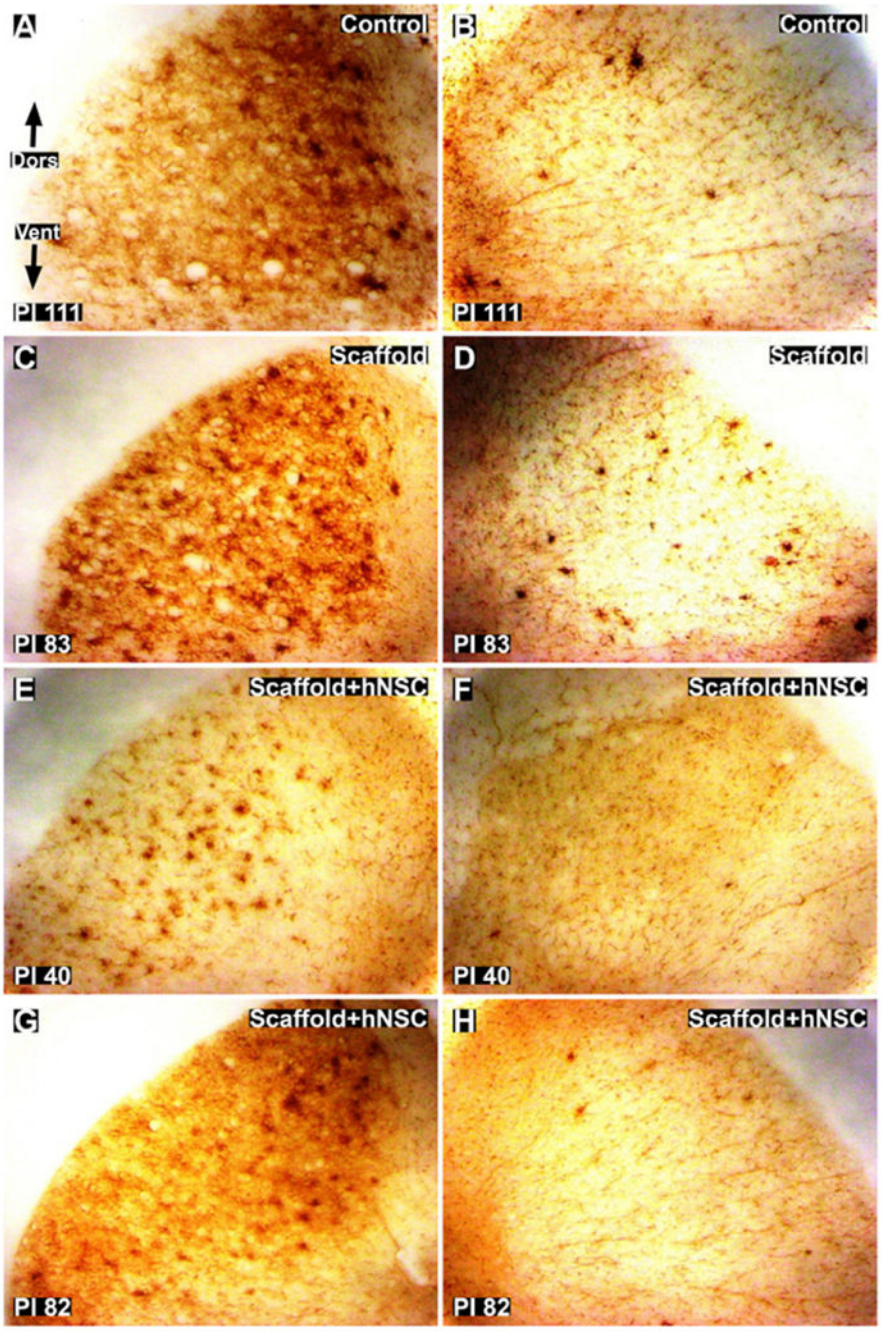

Fig. 11.

Iba1 staining for microglial and macrophage activation around lateral corticospinal tracts (CST) in thoracic cross-sections caudal to the injury site. (A and B): Ipsilateral (A) and contralateral (B) images of control subject 111 days post-injury. (C and D): Ipsilateral (C) and contralateral (D) images of scaffold treated subject 83 days post-injury. E and H: ipsilateral (E and G) and contralateral (F and H) images of scaffold + hNSC treated subjects 40 (E and F) and 82 (G and H) days post-injury. The lesion is unilateral with respect to

microglial and macrophage activation in the cord around the CST. Dors = dorsal. Vent = ventral. Magnification = 10×.

Table 1

Ambulation chamber video observational neuromotor score.

Scale	Description
0	No voluntary function
1	Slight one or two joints movement
2	Active one or two joints, slight movement others
3	Active movement of all three joints, no weight bearing
4	Slight weight bearing, consistent dorsal stepping (no plantar stepping)
5	Slight weight bearing, occasional plantar stepping
6	Frequent plantar stepping, occasional weight bearing, hops with partial weight support
7	Frequent plantar stepping and weight bearing, occasional FL-HL coordination,
8	Consistent plantar stepping and partial weight supported steps, occasional FL-HL coordination
9	Frequent partial weight supported steps, occasional FL-HL coordination
10	Occasional partial weight supported steps, frequent foot drop and/or drag, run with partial weight support
11	Occasional partial weight supported steps, frequent FL-HL coordination
12	Slight partial weight supported steps, frequent FL-HL coordination, stands up HL with partial weight support
13	Slight partial weight supported steps, consistent FL-HL coordination, frequent foot drop and/or drag
14	Full weight supported steps and consistent FL-HL coordination, occasional foot drop and/or drag
15	Occasional foot drop and/or drag, stand up HL with full weight support
16	Slight foot drop and/or drag, no toe clearance
17	No foot drop and/or drag, no toe clearance
18	Occasional toe clearance
19	Frequent toe clearance
20	Normal

Table 2

Study animal summary.

Monkey	Weight (kg)	Sex	Treatment group	Surgery date	Sacrifice date	Sacrifice day
Y464	2.80	M	Scaffold alone	4/19/08	7/11/08	83
X992	2.74	M	Scaffold + hNSC	4/19/08	5/29/08	40
Y156	2.34	M	Control	4/20/08	8/8/08	111
Y430	2.79	M	Scaffold + hNSC	4/20/08	7/11/08	82

Table 3

Quantification of lesion dimensions. All cord widths were normalized to 0.60 cm. All units in cm unless otherwise noted.

Monkey	Treatment group	Sacrifice day	Lesion area (cm^2)	Maximum lesion width
X992	Scaffold + hNSC	40	0.24	0.36
Y430	Scaffold + hNSC	82	0.26	0.28
Y464	Scaffold alone	83	0.26	0.24
Y156	Control	111	0.31	0.29